

Spherical reference cavities for frequency stabilization of lasers in non-laboratory environments

David R. Leibrandt,* Michael J. Thorpe, Mark Notcutt,
Robert E. Drullinger, Till Rosenband, and James C. Bergquist

National Institute of Standards and Technology,
325 Broadway St., Boulder, Colorado 80305, USA

[*david.leibrandt@nist.gov](mailto:david.leibrandt@nist.gov)

Abstract: We present an optical cavity design that is insensitive to both vibrations and orientation. The design is based on a spherical cavity spacer that is held rigidly at two points on a diameter of the sphere. Coupling of the support forces to the cavity length is reduced by holding the sphere at a “squeeze insensitive angle” with respect to the optical axis. Finite element analysis is used to calculate the acceleration sensitivity of the spherical cavity for the ideal geometry as well as for several varieties of fabrication errors. The measured acceleration sensitivity for an initial, sub-ideal version of the mounted cavity is $4.0(5) \times 10^{-11}/g$, $1.6(3) \times 10^{-10}/g$, and $3.1(1) \times 10^{-10}/g$ (where $g = 9.81 \text{ m/s}^2$) for accelerations along the vertical and two horizontal directions, and the fractional frequency stability of a laser locked to the cavity is 1.2×10^{-15} between 0.4 and 13 s. This low acceleration sensitivity combined with the orientation insensitivity that comes with a rigid mount indicates that this cavity design could allow frequency stable lasers to operate in non-laboratory environments.

© 2011 Optical Society of America

OCIS codes: (140.3425) Laser stabilization; (140.4780) Optical resonators; (120.7280) Vibration analysis.

References and links

1. B. C. Young, F. C. Cruz, W. M. Itano, and J. C. Bergquist, “Visible lasers with subhertz linewidths,” *Phys. Rev. Lett.* **82**, 3799–3802 (1999).
2. W. H. Oskay, S. A. Diddams, E. A. Donley, T. M. Fortier, T. P. Heavner, L. Hollberg, W. M. Itano, S. R. Jefferts, M. J. Delaney, K. Kim, F. Levi, T. E. Parker, and J. C. Bergquist, “Single-atom optical clock with high accuracy,” *Phys. Rev. Lett.* **97**, 020801 (2006).
3. B. Willke, K. Danzmann, M. Frede, P. King, D. Kracht, P. Kwee, O. Puncken, R. L. Savage, B. Schulz, F. Seifert, C. Veltkamp, S. Wagner, P. Weßels, and L. Winkelmann, “Stabilized lasers for advanced gravitational wave detectors,” *Class. Quantum Grav.* **25**, 114040 (2008).
4. T. Rosenband, D. B. Hume, P. O. Schmidt, C. W. Chou, A. Brusch, L. Lorini, W. H. Oskay, R. E. Drullinger, T. M. Fortier, J. E. Stalnaker, S. A. Diddams, W. C. Swann, N. R. Newbury, W. M. Itano, D. J. Wineland, and J. C. Bergquist, “Frequency ratio of Al^+ and Hg^+ single-ion optical clocks; metrology at the 17th decimal place,” *Science* **319**, 1808–1812 (2008).
5. K. Numata, A. Kemery, and J. Camp, “Thermal-noise limit in the frequency stabilization of lasers with rigid cavities,” *Phys. Rev. Lett.* **93**, 250602 (2004).
6. D. Kleppner, “Time too good to be true,” *Phys. Today* **59**, 10–11, March (2006).
7. S. Schiller, G. M. Tino, P. Gill, C. Salomon, U. Sterr, E. Peik, A. Nevsky, A. Görlitz, D. Svehla, G. Ferrari, N. Poli, L. Lusanna, H. Klein, H. Margolis, P. Lemonde, P. Laurent, G. Santarelli, A. Clairon, W. Ertmer, E. Rasel, J. Müller, L. Iorio, C. Lämmerzahl, H. Dittus, E. Gill, M. Rothacher, F. Flechner, U. Schreiber, V. Flambaum,

- W.-T. Ni, L. Liu, X. Chen, J. Chen, K. Gao, L. Cacciapuoti, R. Holzwarth, M. P. Heß, and W. Schäfer, "Einstein gravity explorer – a medium-class fundamental physics mission," *Exp. Astron.* **23**, 573–610 (2009).
8. P. Wolf, C. J. Bordé, A. Clairon, L. Duchayne, A. Landragin, P. Lemonde, G. Santarelli, W. Ertmer, E. Rasel, F. S. Cataliotti, M. Inguscio, G. M. Tino, P. Gill, H. Klein, S. Reynaud, C. Salomon, E. Peik, O. Bertolami, P. Gil, J. Páramos, C. Jentsch, U. Johann, A. Rathke, P. Bouyer, L. Cacciapuoti, D. Izzo, P. D. Natale, B. Christophe, P. Touboul, S. G. Turyshev, J. Anderson, M. E. Tobar, F. Schmidt-Kaler, J. Vigué, A. A. Madej, L. Marmet, M.-C. Angonin, P. Delva, P. Tournenc, G. Metris, H. Müller, R. Walsworth, Z. H. Lu, L. J. Wang, K. Bongs, A. Toncelli, M. Tonelli, H. Dittus, C. Lämmerzahl, G. Galzerano, P. Laporta, J. Laskar, A. Fienga, F. Roques, and K. Sengstock, "Quantum physics exploring gravity in the outer solar system: the SAGAS project," *Exp. Astron.* **23**, 651–687 (2009).
 9. M. Notcutt, L.-S. Ma, J. Ye, and J. L. Hall, "Simple and compact 1-Hz laser system via an improved mounting configuration of a reference cavity," *Opt. Lett.* **30**, 1815–1817 (2005).
 10. T. Nazarova, F. Riehle, and U. Sterr, "Vibration-insensitive reference cavity for an ultra-narrow-linewidth laser," *Appl. Phys. B* **83**, 531–536 (2006).
 11. A. D. Ludlow, X. Huang, M. Notcutt, T. Zanon-Willette, S. M. Foreman, M. M. Boyd, S. Blatt, and J. Ye, "Compact, thermal-noise-limited optical cavity for diode laser stabilization at 1×10^{-15} ," *Opt. Lett.* **32**, 641–643 (2007).
 12. S. A. Webster, M. Oxborrow, and P. Gill, "Vibration insensitive optical cavity," *Phys. Rev. A* **75**, 011801 (2007).
 13. S. A. Webster, M. Oxborrow, S. Pugla, J. Millo, and P. Gill, "Thermal-noise-limited optical cavity," *Phys. Rev. A* **77**, 033847 (2008).
 14. J. Millo, D. V. Magalhães, C. Mandache, Y. L. Coq, E. M. L. English, P. G. Westergaard, J. Lodewyck, S. Bize, P. Lemonde, and G. Santarelli, "Ultrastable lasers based on vibration insensitive cavities," *Phys. Rev. A* **79**, 053829 (2009).
 15. Y. N. Zhao, J. Zhang, A. Stejskal, T. Liu, V. Elman, Z. H. Lu, and L. J. Wang, "A vibration-insensitive optical cavity and absolute determination of its ultrahigh stability," *Opt. Express* **17**, 8970–8982 (2009).
 16. Commercial products are identified for technical clarity. Such identification does not imply endorsement by the National Institute of Standards and Technology.
 17. L. Chen, J. L. Hall, J. Ye, T. Yang, E. Zang, and T. Li, "Vibration-induced elastic deformation of Fabry-Perot cavities," *Phys. Rev. A* **74**, 053801 (2006).
 18. T. Legero, T. Kessler, and U. Sterr, "Tuning the thermal expansion properties of optical reference cavities with fused silica mirrors," *J. Opt. Soc. Am. B* **27**, 914–919 (2010).
 19. S. T. Dawkins, R. Chicireanu, M. Petersen, J. Millo, D. V. Magalhães, C. Mandache, Y. Le Coq, and S. Bize, "An ultra-stable referenced interrogation system in the deep ultraviolet for a mercury optical lattice clock," *App. Phys. B* **99**, 41–46 (2010).
 20. R. W. P. Drever, J. L. Hall, F. V. Kowalski, J. Hough, G. M. Ford, A. J. Munley, and H. Ward, "Laser phase and frequency stabilization using an optical resonator," *Appl. Phys. B* **31**, 97–105 (1983).
 21. L. S. Ma, P. Jungner, J. Ye, and J. L. Hall, "Delivering the same optical frequency at two places: accurate cancellation of phase noise introduced by an optical fiber or other time-varying path," *Opt. Lett.* **19**, 1777–1779 (1994).
 22. C. W. Chou, D. B. Hume, J. C. J. Koelemeij, D. J. Wineland, and T. Rosenband, "Frequency comparison of two high-accuracy Al⁺ optical clocks," *Phys. Rev. Lett.* **104**, 070802 (2010).
 23. M. J. Thorpe, D. R. Leibrandt, T. M. Fortier, and T. Rosenband, "Measurement and real-time cancellation of vibration-induced phase noise in a cavity-stabilized laser," *Opt. Express* **18**, 18744–18751 (2010).

1. Introduction

Frequency stable lasers [1] are useful tools with applications in optical frequency standards [2], gravitational wave detection [3], and tests of fundamental physics [4]. Stability is most often achieved by locking the laser to a Fabry-Perot cavity that transfers the length stability of the cavity to frequency stability of the laser. The ultimate stability limit is set by thermomechanical noise [5], but this limit can only be reached when care is taken to suppress the coupling of temperature fluctuations and mechanical vibrations to the cavity length. Thus far, frequency stable lasers have been constrained to operate in low-noise laboratory environments due primarily to vibration and orientation sensitivity. There is growing interest in frequency stable lasers capable of operation outside the laboratory for applications such as geodesy [6] and space based tests of general relativity and fundamental physics [7, 8]. Furthermore, insensitivity to environmental perturbations will be required before frequency stable laser technology can be commercialized.

Recently, several research groups have built cavities that are designed to be vibration insen-

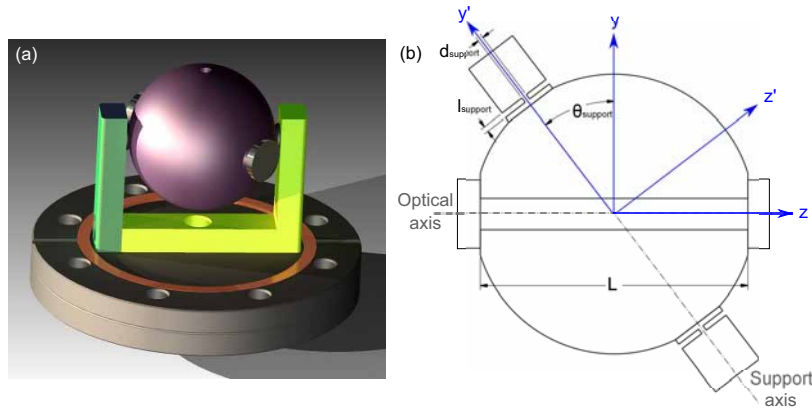


Fig. 1. (a) CAD rendering of a SC mounted at the squeeze insensitive angle with Viton o-ring contacts. Note that this is the experimental design. (b) Cross section of a SC mounted at the squeeze insensitive angle with cylindrical ULE contacts. This is the design used for the finite element analysis model. Important coordinate systems and dimensions are labeled. The sphere is 50.8 mm in diameter and has a 6 mm diameter bore drilled through it along the optical axis. The mirrors are optically contacted to the sphere on flats separated by $L = 48.5$ mm and are 12.7 mm in diameter and 4.2 mm thick. The two support contacts are attached to the sphere along the support axis which is oriented at $\theta_{\text{support}} = 37.31^\circ$ with respect to the y axis and have dimensions $d_{\text{support}} = l_{\text{support}} = 1$ mm.

sitive [9–15]. These designs use symmetries of the cavity spacer to suppress the acceleration sensitivity and hold the spacer with a soft mount that serves to equalize the forces at each support point as well as low-pass filter the vibrations. Often the spacer rests on rubber pads and is held in place by gravity. These cavities have achieved acceleration sensitivities as low as $10^{-10}/g$, but they will not work in a field environment because their mounts are too soft to maintain alignment for accelerations greater than 1 g or changes in orientation with respect to gravity.

In this work, we present an optical cavity design that is insensitive to both vibrations and orientation (see Fig. 1). The cavity spacer is a 50.8 mm diameter sphere made of Corning ultra low expansion (ULE) glass [16], and the mirrors are made of fused silica for reduced thermo-mechanical noise [5]. The high-fold symmetry of the spherical cavity (SC), broken only by fabrication errors and material inhomogeneity, results in a low acceleration sensitivity. Furthermore, the SC is mounted rigidly at two points on a diameter to allow operation at any orientation with respect to gravity.

This paper proceeds as follows. The theoretical performance of the SC is discussed in Section 2, including a finite element analysis study of the contribution of fabrication errors to the acceleration sensitivity. Section 3 presents the experimental setup and some basic diagnostics. The Allan deviation is measured to be within a factor of two of the thermomechanical noise floor of the SC, indicating that the rigid mount does not make a significant contribution. Section 4 presents an experimental measurement of the SC acceleration transfer functions. Finally, Section 5 summarizes and concludes.

2. Theoretical performance

Figure 1 shows a schematic of the SC in its mount. While the rigid mount is essential to allow orientation insensitivity, it is important to choose the location of the contact points between the

mount and the SC such that changes in the squeeze force applied by the mount to the SC (due, for example, to thermal expansion or contraction of the mount) do not couple to the length of the optical axis. If the support axis were orthogonal to the optical axis ($\theta_{\text{support}} = 0$) then an increase in the squeeze force would cause the optical axis to lengthen via Poisson's ratio. If, on the other hand, the support axis were very close to parallel with the optical axis ($\theta_{\text{support}} \sim 90^\circ$) then an increase in the squeeze force would cause the optical axis to contract. We mount the SC at a "squeeze insensitive angle" between the two extremes where there is a zero crossing in the squeeze sensitivity. This squeeze insensitive mounting angle has the additional benefit of decoupling thermomechanical noise in the mount from the length of the optical axis.

Note that the SC geometry allows the possibility of a single spacer with several optical cavities, all of which would be acceleration and orientation insensitive as long as the support axis is on any diameter of the sphere. Furthermore, the optical axes can be oriented on the surface of a cone such that they are all at the squeeze insensitive angle with respect to the support axis.

Ideally, the area of the contact points would be very small so that all of the forces applied by the mount to the SC are applied exactly on a diameter of the sphere. This symmetric configuration reduces the acceleration sensitivity. We consider two different types of contact points in this work. The first type of contact, depicted in Fig. 1(a) and used for all of the experimental results in this paper, is made by squeezing the SC between two DuPont Viton [16] o-rings. We have tried a round cross-section o-ring with a diameter of 4.7 mm and a width of 2.4 mm as well as a rectangular cross-section o-ring with an inner diameter of 2.0 mm, an outer diameter of 5.5 mm, and a thickness of 0.7 mm, and did not see a significant difference in the experimental acceleration sensitivity. The squeeze force is estimated to be of the order of 10 N. This type of contact has the advantage that it is simple to implement but the disadvantage that the area of the support is rather large. The second type of contact, depicted in Fig. 1(b) and used in the finite element model described below, is made by polishing two optical flats on the SC and optically contacting two ULE cylinders to the SC. The cylinders are machined to have a large diameter (~ 1 cm) where they are optically contacted to the SC for a mechanically strong connection, then a short, small diameter section ($d_{\text{support}} \sim l_{\text{support}} \sim 1$ mm) so that all of the forces are applied through a diameter of the SC, then another large diameter (~ 1 cm) section where they are clamped by the mount. The squeeze force could be set to zero for this contact, and a SC mounted with them is expected to survive linear and rotational accelerations of roughly 50 g and 500 rad/s². While this type of contact might not be very practical to implement, it is convenient to model and it captures all the necessary physics of a contact with a very small effective area.

The stiffness of either type of contact can be described in terms of the resonance frequency of the SC vibrating with respect to its mount. The ideal stiffness is a compromise between a stiffness high enough to maintain alignment of the laser to the SC in a vibrationally noisy, orientation changing environment and a stiffness low enough to suppress the coupling of high-frequency vibrations to the sphere. In our experimental implementation of the first type of contact, we cut flexure springs in the mount such that the measured resonance frequency for motion along the support axis is ~ 135 Hz. In the second type of contact, the small diameter section of the ULE cylinders act as flexure springs. For $d_{\text{support}} = l_{\text{support}} = 1$ mm, finite element analysis predicts a single low frequency mode where the sphere rotates around the support axis at ~ 54 Hz, and the modes where the SC moves with respect to the mount are between ~ 1.5 and ~ 2.8 kHz. The mode frequencies can be tailored by modifying the material and geometry of the contact.

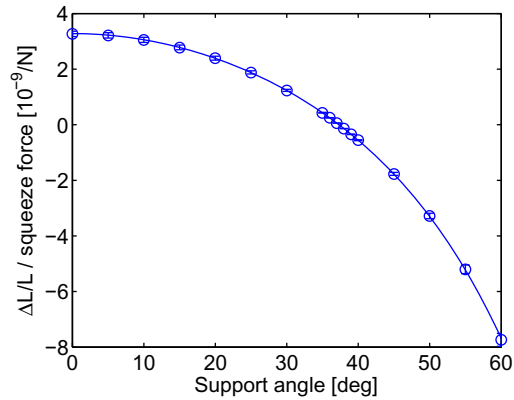


Fig. 2. Calculated sensitivity of the SC length to squeeze force as a function of support angle. The results of the finite element model (markers) are shown along with a fit (line) given by $3.279 - 2.200 \times 10^{-3} \theta^2 - 3.410 \times 10^{-8} \theta^4 - 5.559 \times 10^{-11} \theta^6$ in units of $10^{-9}/\text{N}$. The zero crossing at $37.31(40)^\circ$ is the squeeze insensitive angle where the length of the optical axis of a SC made of ULE is insensitive to squeeze force. The squeeze insensitive angle for fused silica is $37.01(40)^\circ$.

2.1. Finite element model

We performed finite element analysis (FEA) of the SC in order to calculate the squeeze insensitive angle and investigate the effect of different contact geometries and fabrication errors on the acceleration sensitivity. The FEA was calculated by ANSYS [16] with $\approx 250,000$, 10-node tetrahedral elements. The material properties of ULE (density, 2.21 g/cm^3 ; elastic modulus, 67.6 GPa , Poisson's ratio, 0.17) are used for all of the elements. We have verified that there is no significant difference in the squeeze insensitive angle or acceleration sensitivity if the material properties of fused silica are used instead for the mirrors.

2.2. Support angle

Figure 2 shows the calculated sensitivity of the SC length to squeeze force as a function of the support angle. The squeeze insensitive angle is located at $\theta_{\text{support}} \equiv \theta_0 = 37.31(40)^\circ$ where there is a zero crossing in the squeeze sensitivity (for Corning ULE). The uncertainty is dominated by our lack of knowledge of Poisson's ratio in ULE; the discretization error of our FEA model contributes an uncertainty of 0.03° .

2.3. Linear acceleration sensitivity

Vibrations with the largest contribution to the laser phase noise are at low frequency ($\lesssim 100 \text{ Hz}$) compared with the lowest resonance frequency of the SC spacer ($\sim 50 \text{ kHz}$), so it is sufficient to analyze the static case where a gravity-like force is applied to the SC with the outside end surface of each support cylinder fixed in place [17]. We computed the length change of the optical axis for linear accelerations of magnitude $\pm 0.1g$, $\pm g$, and $\pm 10g$ in each direction, where $g = 9.81 \text{ m/s}^2$ is the acceleration due to gravity at the Earth's surface. For each model geometry, the length change is linear in the applied acceleration. The length of the optical axis can change due to either translations or rotations of the two mirrors. To first order in the rotation angles,

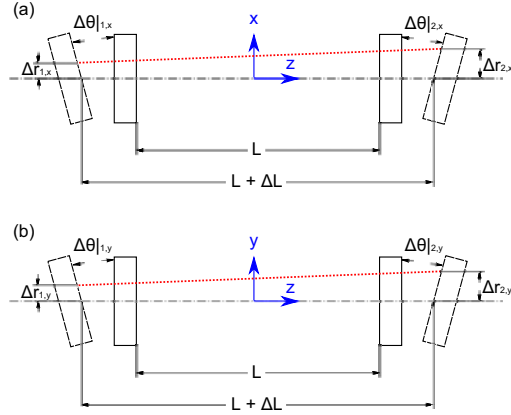


Fig. 3. Schematics showing the deformed positions of the SC mirrors in the (a) $x-z$ and (b) $y-z$ planes. The original positions of the mirrors are drawn in solid lines and the deformed positions are drawn in dashed lines. The optical axis is drawn as a red dotted line. The translational and angular deformations are defined.

the total acceleration sensitivity for acceleration in the α direction is given by

$$\frac{\Delta L}{L} \Big|^\alpha + \sum_{\substack{i \in \{1,2\} \\ \beta \in \{x,y\}}} \frac{\Delta \theta_{i,\beta}^\alpha \Delta r_{i,\beta}}{L}, \quad (1)$$

where $\Delta r_{i,\beta}$ is the displacement of the optical axis from the geometric center of mirror i in the β direction (a fabrication error) and L is the length of the optical axis. The translational and rotational displacements are defined in Fig. 3. The first term in Eq. (1) is the length change of the distance between the geometric centers of the two mirrors and the second term is the length change due to rotation of the mirrors. The first order rotation term in Eq. (1) is zero if the optical mode is centered in the mirrors ($\Delta r_{i,\beta} = 0$). Note that while the length of the optical axis is in fact sensitive to mirror rotations even if it is located perfectly in the center of the mirrors, this effect is of second order and results in a correction to Eq. (1) of

$$\sum_{\beta \in \{x,y\}} \frac{g_2 \left(\theta_{1,\beta}^\alpha \right)^2 + 2\theta_{1,\beta}^\alpha \theta_{2,\beta}^\alpha + g_1 \left(\theta_{2,\beta}^\alpha \right)^2}{2(1 - g_1 g_2)} + \mathcal{O} \left(\left(\theta_{i,\beta}^\alpha \right)^3 \right), \quad (2)$$

where $g_i = 1 - L/R_i$, with R_i the radius of curvature of mirror i . For the cavities we have constructed ($R_1 = 50$ cm, $R_2 = \infty$, worst case mirror rotation acceleration sensitivity $\approx 10^{-8}$ rad/g) this second order correction is of the order of $\approx 10^{-15}/g^2$, which is negligible. However, if the size of the optical mode on the cavity mirrors is made larger by choosing a near-spherical or near-planar design then this correction could become significant.

Tables 1 and 2 show the calculated acceleration sensitivity of the SC for mounting at the squeeze insensitive angle and at $\theta_{\text{support}} = 0$. Each table includes a column for the ideal geometry (column 1) as well as columns for several varieties of fabrication errors. We considered the following types of fabrication errors: supports not on a diameter of the sphere (columns 2 and 3) and flexure springs with unequal stiffness (column 4). For each type we set the error magnitude at a level that we think is attainable. With these levels of fabrication errors, the acceleration sensitivity is roughly $3 \times 10^{-11}/g$ for mounting at either $\theta_{\text{support}} = \theta_0$ or $\theta_{\text{support}} = 0$. For a

SC mounted at $\theta_{\text{support}} = 0$ with unequal stiffness flexure springs, there is a contribution to the acceleration sensitivity due to acceleration induced squeeze forces. This contribution is suppressed at $\theta_{\text{support}} = \theta_0$. However, at the mounting angle of $\theta_{\text{support}} = \theta_0$ the sensitivity to optical axis misalignment is 30 % higher than for $\theta_{\text{support}} = 0$. Practical experience is needed to determine which fabrication errors dominate the residual acceleration sensitivity, and which mounting angle is optimal.

Table 1. Calculated sensitivity of the SC length to accelerations for mounting at the squeeze insensitive angle¹

		Ideal	0.1° off diameter z'	0.1° off diameter x	1 % different springs
	$\Delta L/L _x$	0	-0.1(2)	-1.7(2)	0.0(2)
	$\Delta\theta _{1,x}^x \Delta r_{1,x}/L$	5(1)	5(1)	5(1)	5(1)
	$\Delta\theta _{2,x}^x \Delta r_{2,x}/L$	5(1)	5(1)	5(1)	5(1)
	$\Delta\theta _{1,y}^x \Delta r_{1,y}/L$	0(1)	0(1)	0(1)	0(1)
	$\Delta\theta _{2,y}^x \Delta r_{2,y}/L$	0(1)	0(1)	0(1)	0(1)
	$\Delta L/L _{y'}$	0	7.3(2)	0.0(2)	0.0(2)
	$\Delta\theta _{1,x}^{y'} \Delta r_{1,x}/L$	0(1)	0(1)	0(1)	0(1)
	$\Delta\theta _{2,x}^{y'} \Delta r_{2,x}/L$	0(1)	0(1)	0(1)	0(1)
	$\Delta\theta _{1,y}^{y'} \Delta r_{1,y}/L$	5(1)	5(1)	5(1)	5(1)
	$\Delta\theta _{2,y}^{y'} \Delta r_{2,y}/L$	5(1)	5(1)	5(1)	6(1)
	$\Delta L/L _{z'}$	0	2.4(2)	0.0(2)	0.9(2)
	$\Delta\theta _{1,x}^{z'} \Delta r_{1,x}/L$	0(1)	0(1)	0(1)	0(1)
	$\Delta\theta _{2,x}^{z'} \Delta r_{2,x}/L$	0(1)	0(1)	0(1)	0(1)
	$\Delta\theta _{1,y}^{z'} \Delta r_{1,y}/L$	17(1)	17(1)	17(1)	17(1)
	$\Delta\theta _{2,y}^{z'} \Delta r_{2,y}/L$	17(1)	17(1)	17(1)	17(1)

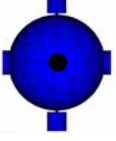
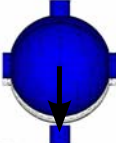
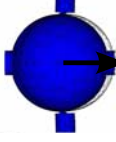
¹Results are presented for the ideal SC geometry shown in Fig. 1(b) as well as for a few varieties of fabrication errors. The columns labeled “0.1° off diameter β ” have the two supports separated by 180.1° in the $\beta - y'$ plane, and the column labeled “1 % different springs” has a 1 % difference in l_{support} between the two supports. The results are given in the form of fractional length change of the optical axis, $\Delta L/L|^\alpha$, and angular tilt of cavity mirror i in the $\beta - z$ plane, $\Delta\theta|_{i,\beta}^\alpha$, for 1 g of acceleration along axis α (see Fig. 3). The fractional length change coefficients are given in units of $10^{-12}/g$, and the angular tilt coefficients are given in units of 10^{-12} rad/g with $\Delta r_{i,\beta} = 100 \mu\text{m}$.

2.4. Rotational velocity and acceleration sensitivity

In a laboratory environment, rotational velocities and accelerations are small in magnitude and have a negligible effect on cavity stability. This may not be the case in some non-laboratory environments. For example, a moving vehicle might experience rotational velocities of $(90^\circ)/(5 \text{ s}) \approx 0.3 \text{ rad/s}$ and rotational accelerations of $g/(2 \text{ m}) \approx 5 \text{ rad/s}^2$.

To estimate how important these effects would be for a SC operating in a non-laboratory environment, we computed the length change of the optical axis of a SC mounted at the squeeze insensitive angle without any fabrication errors for rotational velocities of $\pm 0.1 \text{ rad/s}$, $\pm 1 \text{ rad/s}$, and $\pm 10 \text{ rad/s}$ and rotational accelerations of $\pm 0.1 \text{ rad/s}^2$, $\pm 1 \text{ rad/s}^2$, and $\pm 10 \text{ rad/s}^2$ around each axis. The results are summarized in Table 3. Rotational velocity generates a centrifugal force that is quadratic in velocity, leading to a second order effect on the length of the optical axis. Rotational velocity about an axis orthogonal to the optical axis lengthens the optical

Table 2. Calculated sensitivity of the SC length to accelerations for $\theta_{support} = 0^1$

		Ideal	0.1° off diameter z'	0.1° off diameter x	1 % different springs
	$\Delta L/L ^x$	0	0.0(2)	-7.6(2)	-0.2(2)
	$\Delta\theta _{1,x}^x \Delta r_{1,x}/L$	13(1)	13(1)	13(1)	13(1)
	$\Delta\theta _{2,x}^x \Delta r_{2,x}/L$	13(1)	13(1)	13(1)	13(1)
	$\Delta\theta _{1,y}^x \Delta r_{1,y}/L$	0(1)	0(1)	0(1)	0(1)
	$\Delta\theta _{2,y}^x \Delta r_{2,y}/L$	0(1)	0(1)	0(1)	0(1)
	$\Delta L/L ^y$	0	0.0(2)	0.0(2)	-4.9(2)
	$\Delta\theta _{1,x}^y \Delta r_{1,x}/L$	0(1)	0(1)	0(1)	0(1)
	$\Delta\theta _{2,x}^y \Delta r_{2,x}/L$	0(1)	0(1)	0(1)	0(1)
	$\Delta\theta _{1,y}^y \Delta r_{1,y}/L$	-7(1)	-7(1)	-7(1)	-7(1)
	$\Delta\theta _{2,y}^y \Delta r_{2,y}/L$	-7(1)	-7(1)	-7(1)	-7(1)
	$\Delta L/L ^z$	0	-3.6(2)	0.0(2)	0.0(2)
	$\Delta\theta _{1,x}^z \Delta r_{1,x}/L$	0(1)	0(1)	0(1)	0(1)
	$\Delta\theta _{2,x}^z \Delta r_{2,x}/L$	0(1)	0(1)	0(1)	0(1)
	$\Delta\theta _{1,y}^z \Delta r_{1,y}/L$	0(1)	0(1)	0(1)	0(1)
	$\Delta\theta _{2,y}^z \Delta r_{2,y}/L$	0(1)	0(1)	0(1)	0(1)

¹All other parameters are the same as Table 1.

axis, while rotational velocity about the optical axis shortens the optical axis via Poisson's ratio. Rotational acceleration is less intuitive but our model predicts a small linear sensitivity. The rotational velocity and acceleration estimated above for a moving vehicle applied to the worst case axis (x) would cause a fractional length change of the optical axis of 5×10^{-13} and 1×10^{-12} . Thus, rotational velocity and acceleration will contribute significantly to cavity instability for some non-laboratory environments.

Table 3. Calculated sensitivity of the SC length to rotational velocity and acceleration¹

	Rotational velocity	Rotational acceleration
$\Delta L/L ^x$	5.46 ω_x^2	2.64 $\dot{\omega}_x$
$\Delta L/L ^y$	5.46 ω_y^2	0.00
$\Delta L/L ^z$	-3.19 ω_z^2	0.00

¹Results are presented for the ideal SC geometry shown in Fig. 1(b). The results are given in the form of fractional length change of the optical axis, $\Delta L/L|^{\alpha}$ as a function of rotational velocity, ω_{α} , and rotational acceleration, $\dot{\omega}_{\alpha}$. The fractional length change is given in units of 10^{-12} and have discretization uncertainties of ± 0.05 , where ω_{α} is in units of rad/s and $\dot{\omega}_{\alpha}$ is in units of rad/s².

2.5. Thermal noise

The ultimate stability limit of the SC is set by thermomechanical noise [5]. Our cavity is relatively short, so we use fused silica mirrors to achieve an adequately low thermal noise floor. This

decreases the zero crossing temperature of the cavity coefficient of thermal expansion (CTE) from that of ULE (≈ 15 °C for the present cavities) to ≈ -25 °C, but ULE rings optically contacted to the back of the mirrors could be used to bring the CTE zero crossing of the cavity back up to a more manageable temperature [18, 19]. Using the analytic formulas provided in Reference [5] we calculate a thermal noise floor limited Allan deviation of 6.5×10^{-16} , dominated by noise from the mirror coatings. FEA suggests that the contribution from the rigid mount is negligible for mounting at either the squeeze insensitive angle or at $\theta_{\text{support}} = 0$.

3. Experimental setup

A schematic of the experimental setup is shown in Fig. 4. The SC is mounted in a vacuum chamber inside a heat shield that is stabilized to the cavity CTE zero crossing temperature. The mount is made of invar. A test laser is locked to the SC by the PDH method [20] via fast feedback to an AOM and slow feedback to a piezo in the laser cavity. The vacuum chamber and test laser are located on an active vibration isolation (AVI) table, along with a three axis accelerometer mounted to the SC vacuum chamber. The AVI table can be driven in order to measure the SC acceleration sensitivity. The phase of the test laser is measured via a heterodyne beat note with a second frequency stable laser (reference laser), which is completely independent and located in a separate room. The reference laser comes through a noise canceled fiber [21] and is beat against the test laser on a fast photodiode. This beat note is first mixed down to about 6 MHz, then further mixed to near 0 Hz using a demodulator circuit that outputs the in-phase (I) and quadrature (Q) components of the signal. The I and Q components are recorded with an analog-to-digital converter (ADC) at a sample rate of 1 to 100 kHz.

We built two nearly identical SC setups, with the primary difference being that they use different wavelength test lasers and are compared with different reference lasers. The first setup uses a fiber laser that is frequency doubled to 563 nm as the test laser and a laser that typically serves as the clock laser for probing the $^2S_{1/2}$ to $^2D_{5/2}$ transition in $^{199}\text{Hg}^+$ [2] as the reference laser. This setup was used for the diagnostics presented in this section. The second setup uses a fiber laser at 1070 nm as the test laser and a laser that typically serves as the clock laser for probing the 1S_0 to 3P_0 transition in $^{27}\text{Al}^+$ [22] as the reference laser. This setup was used for the acceleration sensitivity measurements presented in Section 4.

As a validation test of our FEA model, we measured the sensitivity of the SC length to squeeze force at $\theta_{\text{support}} = 0$ and at $\theta_{\text{support}} = \theta_0$. The measurement is performed by modulating the squeeze force at 20 Hz with a piezo located between one of the o-ring contacts and the mount and looking at the resulting length change of the optical axis with a lock-in technique. At $\theta_{\text{support}} = \theta_0$, we observe a factor of approximately 100 reduction and a sign change in the squeeze sensitivity. This is in qualitative agreement with our FEA model.

The Allan deviation of the 563 nm laser locked to the first SC is shown in Fig. 5. The Allan deviation is roughly flat at 1.2×10^{-15} between 0.4 and 13 s. This is about a factor of two higher than our theoretical estimate of the thermal noise floor, 6.5×10^{-16} .

4. Acceleration sensitivity and cavity transfer functions

We measured the acceleration sensitivity of the SC by driving the AVI table and recording the resulting acceleration of the SC vacuum chamber and phase excursion of the test laser. We performed measurements with three different AVI drive directions at each drive frequency. For each drive frequency and direction, the measured laser frequency and acceleration are Fourier transformed and the components at the drive frequency are used to determine the acceleration sensitivity for acceleration along some direction. Since the AVI table shows a strong, frequency dependent coupling between drive axes our three measurements of the acceleration sensitivity at each frequency are along three non-orthogonal directions, but (since the three measured

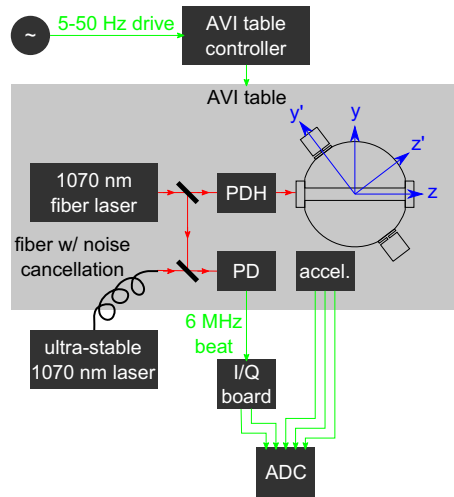


Fig. 4. Schematic of the experimental setup used to measure the SC acceleration sensitivity. The setup used to measure the SC support squeeze sensitivity and Allan deviation is identical, except that the 1070 nm lasers are replaced by 563 nm lasers. The SC is mounted in a vacuum chamber located on an AVI table. A 1070 nm fiber laser is locked to the SC by the PDH method via fast feedback to an AOM and slow feedback to a piezo in the laser cavity. The phase of the laser is measured via a heterodyne beat note with a second (completely independent and located in a separate room) frequency stable 1070 nm laser. The beat note is mixed down to 6 MHz, fed into an I/Q demodulator circuit, and recorded with an ADC at a sample rate of 1 to 100 kHz. The AVI table drives accelerations at frequencies of 5 to 50 Hz, and a three axis accelerometer mounted on the SC vacuum chamber measures the applied accelerations.

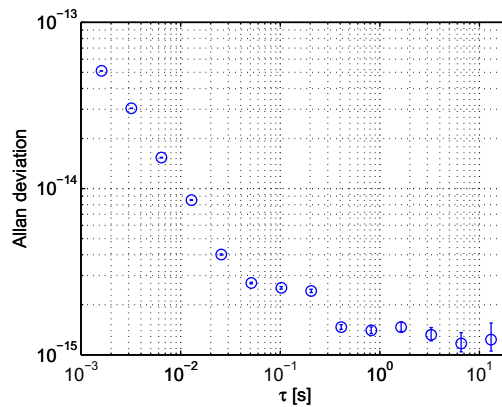


Fig. 5. Allan deviation of the SC calculated from a 200 s phase measurement. A 1.8 Hz/s linear frequency drift is removed in the data analysis before calculating the Allan deviation. The Allan deviation is roughly flat at 1.2×10^{-15} between 0.4 and 13 s.

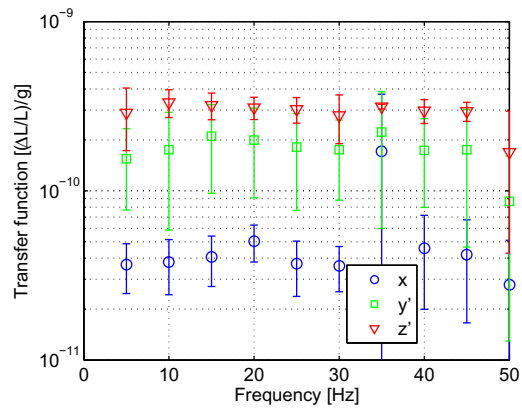


Fig. 6. Measured SC acceleration sensitivity as a function of frequency. The transfer function for accelerations along each axis are given in units of fractional length change per g. The mean acceleration sensitivities are $4.0(5) \times 10^{-11}/g$ for accelerations along the x axis, $1.6(3) \times 10^{-10}/g$ for accelerations along the y' axis, and $3.1(1) \times 10^{-10}/g$ for accelerations along the z' axis.

drive directions at each frequency are non-degenerate) these measurements are easily inverted to obtain the SC acceleration transfer functions for three orthogonal acceleration directions. The results are shown as a function of drive frequency in Fig. 6. The data points and error bars are the mean and standard deviation of five datasets taken with the accelerometer located at three different positions on the SC vacuum chamber. The mean acceleration sensitivities are $4.0(5) \times 10^{-11}/g$ for accelerations along the x axis, $1.6(3) \times 10^{-10}/g$ for accelerations along the y' axis, and $3.1(1) \times 10^{-10}/g$ for accelerations along the z' axis.

The acceleration sensitivity measured for a SC mounted with Viton o-ring contacts is one or two orders of magnitude larger than the acceleration sensitivity calculated by use of FEA for a SC mounted with ULE contacts. We have measured the displacement of the optical mode from a diameter of the sphere to be given by $(\Delta r_{1,x} + \Delta r_{2,x})/2 = 70(60) \mu\text{m}$ and $(\Delta r_{1,y} + \Delta r_{2,y})/2 = 10(50) \mu\text{m}$, which is not large enough to account for the observed acceleration sensitivity. Our hypothesis is that this difference can be attributed to the large effective area of the o-ring contacts. If there is some stress in the o-rings such that the forces applied by the mount to the SC are applied primarily through one side of the o-rings then this situation would be similar to the FEA model we ran where the supports are not on a diameter of the SC, except that the magnitude of the “fabrication error” could be up to two orders of magnitude larger ($\sim 10^\circ$ if the forces were applied all the way at the edge of the o-ring) than what we considered in the FEA model.

5. Conclusion

We have presented a new frequency stable optical cavity design that is insensitive to both vibrations and orientation. Acceleration sensitivity is suppressed by the symmetric spherical spacer geometry, and the cavity is rigidly mounted to allow orientation insensitivity. Mounting at a squeeze insensitive angle eliminates the coupling of the support forces to the length of the optical axis. Experimental measurements have demonstrated stability within a factor of two of the thermal noise floor and acceleration sensitivities of $4.0(5) \times 10^{-11}/g$, $1.6(3) \times 10^{-10}/g$, and $3.1(1) \times 10^{-10}/g$ for accelerations along the vertical and two horizontal directions. FEA mod-

eling suggests that with a smaller area support contact, we may be able to achieve acceleration sensitivities as low as $\approx 3 \times 10^{-11}/\text{g}$ in all directions for experimentally feasible fabrication errors. Combined with new techniques for real-time cancellation of vibration induced phase noise [23], the spherical reference cavities presented here may enable frequency stable lasers to operate with thermomechanical noise limited performance in a non-laboratory environment.

Acknowledgments

We would like to acknowledge critical comments and strong support from R. Lalezari and colleagues at AT Films as well as fruitful discussions with M. Lauer. H. Guan helped with assembly of the SC vacuum system. We thank W. Swann and R. Fox for critical readings of this manuscript, and acknowledge partial support from ONR. D. R. Leibrandt and M. J. Thorpe acknowledge support from the National Research Council. This work is not subject to U.S. copyright.